the conclusion that $R(E)$ and $R(A_1)$ have the same sign, with consequent reinforcement rather than the cancellation seen in solution.

Conclusions. Although there is a great deal of uncertainty about the conformational geometry of $[Cr(en)_3]^{3+}$ in solution and in a $2[Cr(en)_3]Cl_3 \cdot KCl \cdot 6H_2O$ host, the controversy generated by seemingly contradictory assignments for the $^2T_{1g}$ components in the two environments appears to be largely illusory. There is a high probability that both interpretations are correct. Assuming that the bite and twist angles are approximately the same in solution and in the solid state and that the *lel*$_2$*ob* conformational geometry obtains in both cases (although the nitrogen atoms are still assumed to have D_3 symmetry around the Cr in solution), a $^2T_{1g}$ splitting of approximately 150 cm^{-1} and a ^2E_g splitting of about 5 cm^{-1} are to be expected in solution. Since the two $^2T_{1g}$ peaks have opposite signs, a 150-cm^{-1} $^2T_{1g}$ splitting can easily be reconciled with the 300-cm^{-1} peak separation observed by Kaizaki[33] and by Richardson[23] in CD spectra. In the solid state, the deviations of the nitrogen atoms from D_3 symmetry lead to a larger ^2E_g splitting, but a smaller $^2T_{1g}$ splitting, as observed by Güdel.[25] In addition, the axial CD spectrum measured on single crystals results in positive signs for all five $\{^2E_g, ^2T_{1g}\}$ components, while the solution CD spectrum exhibits a mix of signs.

Acknowledgment. This material is based upon work supported in part by the National Science Foundation under Grant RII8610675. We also thank the donors of the Petroleum Research Fund, administered by the American Chemical Society, for their support of this research. I would also like to thank Prof. Lyle Parker for many enlightening discussions.

Contribution from the Chemistry Department, University of Canterbury, Christchurch 1, New Zealand, and Research School of Chemistry, Australian National University, P.O. Box 4, Canberra, ACT 2601, Australia

Vibrational Raman Spectra of Tris(1,2-ethanediamine) Complexes of Cobalt(III) and Rhodium(III)

Bryce E. Williamson,*[†] Lucjan Dubicki,*[‡] and Sven E. Harnung[§]

Received February 17, 1988

Polarized, single-crystal Raman spectra of the complexes $2[Co(en)_3]Cl_6 \cdot NaCl \cdot 6H_2O$ and $2[Rh(en)_3]Cl_6 \cdot KCl \cdot 6H_2O$ have been measured in the region 150–600 cm^{-1}. Assignments are made with the aid of a simplified normal-coordinate analysis calculation. The resonance Raman excitation profiles of $Co(en)_3^{3+}$ in the vicinity of the $^1T_1 \leftarrow {}^1A_1$ electronic transition have been reinvestigated, and the phenomenon of resonance deenhancement is confirmed. An analysis based on the error function model indicates that the observed deenhancement requires the displacements of the two interfering excited states to be in the *same* direction with respect to the ground state.

1. Introduction

Metal chelates of 1,2-ethanediamine (en) have been the subject of numerous investigations. In many cases they form uniaxial crystals that are suitable for a spectroscopic study of optical activity.[1,2] The metal chelates display extensive vibronic activity in the absorption,[1,3–7] emission,[6,7] and circular dichroism[1,3,4,6] spectra.

Although the vibrational spectra have been studied by many authors,[6,8–15] some of the assignments in the MN_6 skeletal region have remained controversial. Recently, a full normal-coordinate analysis of $Rh(en)_3^{3+}$ was made by Borch et al.[14–16] Unfortunately, their work contains errors in the E symmetry coordinates and some of the assignments of the E vibrations must be incorrect.

The Co(III) complexes of en[13] and other polyamine ligands, such as tacn[17] and sepulchrate,[17] exhibit deenhancement in the resonance Raman excitation profiles (RREP) of A_1 vibrations for excitation into the $^1T_1 \leftarrow {}^1A_1$ electronic transition. This effect has been interpreted as an interference between resonance scattering with the $^1T_1$ state and preresonance scattering from a charge-transfer state.[13,18] Previous analysis was restricted to the physically unrealistic case where only a single A_1 vibration was vibronically active and gave the result that the charge-transfer state was compressed along the A_1 coordinate.[18]

In this work we examine the skeletal vibrations of $Co(en)_3^{3+}$ and $Rh(en)_3^{3+}$ using polarized, single-crystal Raman spectroscopy. The symmetry coordinates are corrected, and a simplified normal-coordinate calculation is used to assign the vibrations. The resonance deenhancement of the RREP in $Co(en)_3^{3+}$ is confirmed. Contrary to earlier work,[18] we deduce that the charge-transfer state involved in preresonance scattering is expanded along the a_{1g} breathing coordinate.

2. Experimental Section

Preparation of Crystals. Crystals of (+)-$2[Co(en)_3]Cl_6 \cdot NaCl \cdot 6H_2O$ and (±)-$2[Co(en)_3]Cl_6 \cdot NaCl \cdot 6H_2O$, denoted hereafter as +Co and ±Co, respectively, were available from earlier studies.[1]

Two types of crystals of $Rh(en)_3^{3+}$ were examined spectroscopically, 15% (+)-$Cr(en)_3^{3+}$ and 1–2% (±)-$Cr(en)_3^{3+}$, both doped in the racemic host (±)-$2[Rh(en)_3]Cl_6 \cdot KCl \cdot 6H_2O$.

The 15% sample, denoted hereafter as ±Rh, was prepared by mixing 15.2 g of (+)-$[Rh(en)_3]Cl_3$ in 30 mL of H_2O and 15 g of (+)-$[Cr(en)_3]Cl_3$ in 35 mL of H_2O, at 50 °C. After cooling and filtration, the precipitate was washed with ice-cold H_2O. The precipitate, 29.8 g, and 16 g of (±)-$[Rh(en)_3]Cl_3$ were dissolved in 350 mL of H_2O at 35 °C, and 156 mL of saturated KCl, 452 mL of H_2O, and 32 mL of 4 M HCl were added. The filtered solution was placed in a thermostat at 32 °C. The

[†] University of Canterbury.
[‡] Australian National University.
[§] Chemistry Department I, University of Copenhagen, Denmark.

(1) Dubicki, L.; Ferguson, J.; Geue, R. J.; Sargeson, A. M. *Chem. Phys. Lett.* **1980**, *104*, 393–7.
(2) Dubicki, L.; Ferguson, J.; Williamson, B. *J. Phys. Chem.* **1984**, *88*, 4254–8.
(3) Dingle, R. *Chem. Commun.* **1965**, 304–5.
(4) Denning, R. G. *Chem. Commun.* **1967**, 120–1.
(5) Flint, C. D.; Mathews, A. P. *Inorg. Chem.* **1975**, *14*, 1219–20.
(6) Geiser, U.; Guedel, H. U. *Inorg. Chem.* **1981**, *20*, 3013–9.
(7) McCarthy, P. J.; Vala, M. T. *Mol. Phys.* **1973**, *25*, 17–34.
(8) Powell, D. B.; Sheppard, N. *Spectrochim. Acta* **1961**, *17*, 68–76.
(9) Krishnan, K.; Plane, R. A. *Inorg. Chem.* **1966**, *5*, 852–7.
(10) Gouteron-Vaissermann, J. *C. R. Seances Acac. Sci., Ser. B* **1972**, *275*, 149–50.
(11) James, D. W.; Nolan, M. J. *Inorg. Nucl. Chem. Lett.* **1973**, *9*, 319–29.
(12) Gouteron, J. *J. Inorg. Nucl. Chem.* **1976**, *38*, 63–71.
(13) Stein, P.; Miskowski, V.; Woodruff. W. H.; Griffin, J. P.; Werner, K. G.; Gaber, B. P.; Spiro, T. G. *J. Chem. Phys.* **1976**, *64*, 2159–67.
(14) Borch, G.; Klaboe, P.; Nielsen, P. H. *Spectrochim. Acta, Part A* **1978**, *34A*, 87–91.
(15) Borch, G.; Gustavsen, J.; Klaboe, P.; Nielsen, P. H. *Spectrochim. Acta, Part A* **1978**, *34A*, 93–99.
(16) Borch, G.; Nielsen, P. H.; Klaboe, P. *Acta Chem. Scand., Ser. A* **1977**, *A31*, 109–19.
(17) Williamson, B. E.; Dubicki, L., unpublished results.
(18) Zgierski, M. Z. *J. Raman Spectrosc.* **1977**, *6*, 53–6.

0020-1669/88/1327-3484$01.50/0

temperature was gradually lowered to 15 °C over 10 days, and large hexagonal crystals of (±)-2$[Rh(en)_3]Cl_6 \cdot KCl \cdot 6H_2O$ were formed. The content of (+)-$Cr(en)_3^{3+}$ was ~15%, as determined by atomic absorption. The crystals were invariably strained and often cracked after cooling to 10 K and warming back to 295 K.

The second set of crystals was prepared by mixing 15 g of (±)-2$[Rh(en)_3]Cl_6 \cdot KCl \cdot 6H_2O$, 2 g of (±)-$[Rh(en)_3]Cl_3$, 5.3 g of (±)-2$[Cr(en)_3]Cl_6 \cdot KCl \cdot 6H_2O$, and 40 mL of H_2O with 135 mL of a mixture formed from 78 mL of saturated KCl, 16 mL of 4 M HCl, and 226 mL of H_2O. The content of the racemic impurity, (±)-$Cr(en)_3^{3+}$, was found to be 1% and 2% in two samples.

Crystals suitable for axial and orthoaxial spectroscopic measurements were cut with a rotating wet-fiber instrument, fabricated in the Research School of Chemistry, ANU.

N-deuteriated (d_{12}) crystals were prepared by recrystallization from D_2O. The ^1H NMR and Raman spectra showed that amino deuteriation was complete and the substitution of methylene hydrogen atoms was negligible.

Crystal Structures. Crystals of +Co have the space group $P3$ (C_3^1) with $Z = 1$.[19] The unit cell contains two complex ions centered at inequivalent C_3 sites. The inequivalence at 295 K is very small, and the space group is approximately $P6_3$ (C_6^6). Precession X-ray photographs taken at ~135 K show that the unit cell remains essentially unchanged except for a small contraction; $a = 11.47$ Å and $c = 8.06$ Å at 295 K,[19] and $a = 11.34$ Å and $c = 8.05$ Å at ~135 K.

The racemic crystals, ±Co and ±Rh, are isostructural. The space group is $P\bar{3}c1$ (D_{3d}^4), and $Z = 2$.[20] In this case the unit cell has four complex ions centered at equivalent C_3 sites. Unfortunately, the full X-ray structure has not been determined. It is expected to be similar to the known structure of (±)-$[Co(en)_3]Cl_3 \cdot 3H_2O$, which has the same space group and $Z = 4$.[21]

Spectroscopic Measurements. The Raman equipment has been described elsewhere.[22] The RREP were obtained for a 0.1 M aqueous solution of ±Co contained in a thin-walled soda-glass capillary. The Raman spectra were excited by a Spectra-Physics 165 argon ion laser. Integrated intensities were calibrated in the same manner as described by Stein et al.[13] The Zeeman and emission spectra will be reported elsewhere.

3. Results

3.1. Normal-Coordinate Analysis. The vibrational calculations employed the Wilson **GF** matrix method[23] and were similar to those of Borch et al.[16] except for a number of modifications described below. Reference 16 should be consulted for the detailed description of the internal coordinates.

The $M(en)_3^{3+}$ complex was treated as a 37-body problem with D_3 symmetry. The vibrations then belong to three species with A_1, A_2, and E symmetries. The A_1 and A_2 coordinates were taken from Borch et al.[16] However, the choice of E coordinates requires more care. The trigonal and cubic axes adopted in this paper and in ref 16 follow those of Sugano et al.[24] Hence, the trigonal Z axis lies along the [111] direction, and for the Δ configuration, the trigonal Y axis bisects an angle subtended by a chelate ring. The u and v components of an E representation then transform under D_3 rotations as given in (1).

	$C_3(Z)$	$C_2(Y)$	
S_u	$-(1/2)S_u + (\sqrt{3}/2)S_v$	$+S_u$	(1)
S_v	$-(\sqrt{3}/2)S_u - (1/2)S_v$	$-S_v$	

The required set of E coordinates should transform as one of the components in (1). Most of the E coordinates in ref 16 transform as S_u. However the E coordinates S_{24}, S_{25}, S_{28}, S_{29}, S_{32}, S_{33}, S_{36}, S_{37}, S_{44}, and S_{46} transform as S_v. Of these coordinates, the first eight correspond to rock (NH_2), twist (NH_2), rock (CH_2), and twist (CH_2) modes. In this work they have been replaced by the u components, which are given in Table I.

Table I. Symmetry Coordinates for $M(en)_3^{3+}$ [a]

E_u Ligand Coordinates

$S_{24} = (1/\sqrt{6})[2S_m(I) - S_m(II) - S_m(III)]$ $S_{25} = (1/\sqrt{2})[S_m'(II) - S_m'(III)]$

$S_{28} = (1/\sqrt{6})[2S_o(I) - S_o(II) - S_o(III)]$ $S_{29} = (1/\sqrt{2})[S_o'(II) - S_o'(III)]$

$S_{32} = (1/\sqrt{6})[2S_q(I) - S_q(II) - S_q(III)]$ $S_{33} = (1/\sqrt{2})[S_q'(II) - S_q'(III)]$

$S_{36} = (1/\sqrt{6})[2S_s(I) - S_s(II) - S_s(III)]$ $S_{37} = (1/\sqrt{2})[S_s'(II) - S_s'(III)]$

MN_6 Skeletal Coordinates[b]

$S_1(A_1,a_{1g}) = (1/\sqrt{3})[S_a(I) + S_a(II) + S_a(III)]$

$S_{23}(A_1,t_{2g\tau}) = (1/2\sqrt{3})[\sum_{i=1}^{3}(\theta_i + \theta_i^\circ) + \sum_{i=1}^{6}\phi_i]$

$S_{24}(A_1,t_{2u\tau}) = (1/\sqrt{6})\sum_{i=1}^{3}(\theta_i - \theta_i^\circ)$

$S_{25}(A_1)$ redundant

$S_1(A_2,t_{1uZ}^b) = (1/\sqrt{3})[S_a'(I) + S_a'(II) + S_a'(III)]$

$S_{31}(A_2,t_{1uZ}^a) = (1/\sqrt{6})[\phi_1 - \phi_2 + \phi_3 - \phi_4 + \phi_5 - \phi_6]$

$S_1(E_u,e_{gu}) = (1/2\sqrt{3})[2L_1(II) + 2L_2(III) - L_1(III) - L_2(I) - L_1(I) - L_2(II)]$

$S_2(E_u,t_{1uY}^b) = (1/2)[L_1(I) - L_2(II) + L_2(I) - L_1(III)]$

$S_{43}(E_u,t_{1uY}^a) = (1/4)[\phi_4 + \phi_5 - \phi_3 - \phi_6 - 2\theta_1 + \theta_2 + \theta_3 + 2\theta_1^\circ - \theta_2^\circ - \theta_3^\circ]$

$S_{44}(E_u,t_{2g\rho}) = (1/2\sqrt{6})[2\phi_1 + 2\phi_2 - \phi_4 - \phi_5 - \phi_3 - \phi_6 - 2\theta_1 + \theta_2 + \theta_3 - 2\theta_1^\circ + \theta_2^\circ + \theta_3^\circ]$

$S_{45}(E_u,t_{2u\rho}) = (1/4\sqrt{3})[3\phi_3 + 3\phi_6 - 3\phi_4 - 3\phi_5 - 2\theta_1 + \theta_2 + \theta_3 + 2\theta_1^\circ - \theta_2^\circ - \theta_3^\circ]$

$S_{46}(E_u)$ redundant

[a] The table lists the coordinates that have been modified, as described in the text. The remaining coordinates, as well as a full description of the notation, is given in ref 16. The labels I, II, and III refer to the chelate rings. [b] The trigonal coordinates were obtained from the cubic set as described in the text.

Table II. Force Constants for $M(en)_3^{3+}$

force const[a]	$Co(en)_3^{3+}$	$Rh(en)_3^{3+}$	units
K_L	1.740	2.060	mdyn·Å^{-1}
F_{LL}	0.070	0.057	
F_{LL}'	0.210	0.437	
$F_{L\omega}$	0.200	0.216	mdyn·rad^{-1}
H_ω	0.440[b]	0.755	mdyn·Å·rad^{-2}
$H_\theta = H_\phi$	1.096	1.077	
$F_\theta = F_\phi$	0.000	0.000	
$F_\theta' = F_\phi'$	0.138	0.251	

[a] The choice of force constants in this table is described in the text. Other force constants are given in Table 2 of ref 16. [b] Taken from: Bigotto, A.; Costa, G.; Galasso, V.; De Alti, G. *Spectrochim. Acta, Part A* **1970**, *26A*, 1939–49.

We have also replaced the MN_6 coordinates of ref 16 by the trigonally adapted coordinates of the octahedral parent, in order to make the contributions from the MN_6 skeleton more transparent (Table I). The latter were derived from the cubic set by using (2).

$$\begin{bmatrix} T_{X,\rho} \\ T_{Y,\sigma} \\ T_{Z,\tau} \end{bmatrix} = \frac{1}{\sqrt{6}} \begin{bmatrix} -1 & -1 & 2 \\ \sqrt{3} & -\sqrt{3} & 0 \\ \sqrt{2} & \sqrt{2} & \sqrt{2} \end{bmatrix} \begin{bmatrix} T_{x,\xi} \\ T_{y,\eta} \\ T_{z,\zeta} \end{bmatrix} \quad (2)$$

In D_3 symmetry, T_{1Z} and $T_{2\tau}$ transform as A_2 and A_1, respectively, and the bases (E_u, E_v), ($T_{2\rho}$, $T_{2\sigma}$), and (T_{1Y}, $-T_{1X}$) follow the standard transformations in (1).

The Cartesian coordinates for heavy atoms were taken from Nakatsu et al.[19] The hydrogen positions were determined in the same way as given in ref 16. The ligand force constants were also taken from ref 16, since the vibrational frequencies below 600 cm^{-1} are only weakly dependent on the force constants of the amine and ethylene groups. The MN_6 force constants (Table II) were

(19) Nakatsu, K.; Shiro, M.; Saito, Y.; Kuroya, H. *Bull. Chem. Soc. Jpn.* **1957**, *30*, 158–64.
(20) Dingle, R.; Ballhausen, C. J. *Mat.-Fyz. Medd.—K. Dan. Vidensk. Selsk.* **1967**, *35*, 1–26.
(21) Nakatsu, K.; Saito, Y.; Kuroya, H. *Bull. Chem. Soc. Jpn.* **1956**, *29*, 428–34.
(22) Johnstone, I. W.; Dubicki, L. *J. Phys. C* **1980**, *13*, 121–30.
(23) Wilson, E. B.; Decius, J. C.; Cross, P. C. *Molecular Vibrations*; McGraw-Hill: New York, 1955; pp 74–6.
(24) Sugano, S.; Tanabe, Y.; Kamimura, H. *Multiplets of Transition Metal Ions in Crystals*; Academic: New York, 1970.

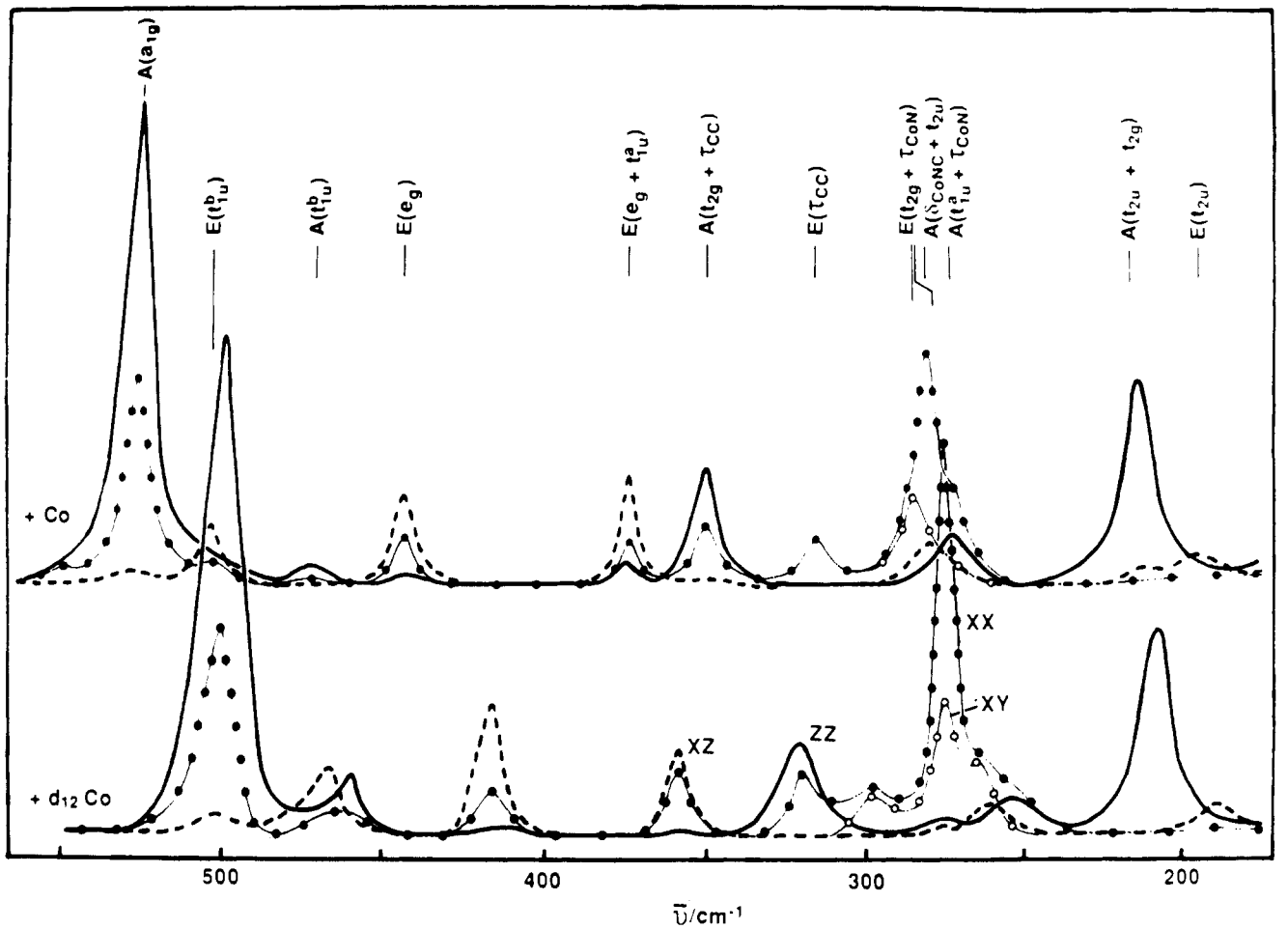

Figure 1. Raman spectra of (+)-2[Co(en)$_3$]Cl$_6$·NaCl·6H$_2$O (+Co) and its N-deuteriated (d_{12}) analogue (+Co-d_{12}) at 320 K. The *XY* spectra are omitted outside the region 240–320 cm^{-1}. I_{XY} is very small for A bands, and $I_{XY} = I_{XX}$ for all E bands. The bands are labeled according to the symmetry species of the C_3 factor group with the predominant MN_6 skeletal and ligand coordinates indicated in parentheses. Similar notation is used in Figures 3 and 4.

Table III. Correlation Table for MN_6 Coordinates of M(en)$_3^{3+}$

MN_6 parentage O_h	M(en)$_3^{3+}$ free ion D_3	M(en)$_3^{3+}$ site C_3	+Co factor group C_3	+Co pseudo factor group C_6	±Co, ±Rh factor group D_{3d}
a_{1g}	A_1	A	2A	A + B	$A_{1g} + A_{2g} + A_{1u} + A_{2u}$
e_g	E	E	2E	$E_1 + E_2$	$2E_g + 2E_u$
t_{1u}^a, t_{1u}^b	$A_2 + E$	A + E	2A + 2E	$A + B + E_1 + E_2$	$A_{1g} + A_{2g} + A_{1u} + A_{2u} + 2E_g + 2E_u$
t_{2g}, t_{2u}	$A_1 + E$	A + E	2A + 2E	$A + B + E_1 + E_2$	$A_{1g} + A_{2g} + A_{1u} + A_{2u} + 2E_g + 2E_u$

Raman activity: A, A_1, A_{1g} ($XX = YY$, ZZ); E, E_g ($XX = YY = XY$, $XZ = YZ$); E_1 ($XZ = YZ$), E_2 ($XX = YY = XY$).

obtained from the analyses of the vibrational frequencies for [Rh(NH$_3$)$_6$]Cl$_3$[25] and [Co(NH$_3$)$_6$]I$_3$.[26,27] The t_{2u} modes for these complexes are both Raman and infrared inactive, and their frequencies have not been measured. Del Rey and Hase[28] have calculated $\bar{\nu}(t_{2u}) \approx 182$ cm^{-1} for Co(NH$_3$)$_6^{3+}$, while the value determined for Cr(NH$_3$)$_6^{3+}$ from emission studies[29] is $\bar{\nu}(t_{2u}) = 230$ cm^{-1}. Our results are qualitatively insensitive to the variation of the frequency between these two limits, and the results presented here were obtained by using $\bar{\nu}(t_{2u}) = 230$ cm^{-1} for both complexes.

Calculated frequencies were obtained without reference to observed values, and we do not expect them to give excellent agreement with the experimental frequencies. However, we expect our restricted model to account for the major trends and frequency shifts of the spectra. Since the force constants are fixed, our results should not be distorted by a priori assignments or erroneous selections of "observed" frequencies (section 4.1).

3.2. Raman Spectra. The 320 K Raman spectra of +Co and +Co-d_{12} are given in Figure 1. The symmetry species of the C_3 site group are readily assigned from the polarization data. Each vibration in the free complex ion should give two bands in the single-crystal spectrum of +Co (Table III). This doubling is not clearly resolved in the 320 K spectra, but it is more apparent at lower temperatures, particularly for the A bands at 530 and 280 cm^{-1} (Figures 2 and 3).

The racemic compounds ±Co and ±Rh should exhibit only one band for each mode of A_1 or A_2 parentage (Table III). This is demonstrated in Figure 3, which gives the 50 K spectra of +Co and ±Co, and in Figure 4, which gives the 295 K spectrum of ±Rh.

The experimental and calculated frequencies and deuteriation shifts are listed in Tables IV and V. The coordinates of the MN_6 skeleton are designated by their O_h parentage, and the notation for the ligand coordinates follows that of Borch et al.[16] The

(25) Griffiths, W. P. *J. Chem. Soc. A* **1966**, 899–901.
(26) Dubicki, L.; Williamson, B. *Inorg. Chem.* **1984**, *23*, 3779–84.
(27) Williamson, B. E. Ph.D. Dissertation, Australian National University, 1983.
(28) Del Rey, M.; Hase, Y. *An. Acad. Bras. Cienc.* **1979**, *51*, 87–92.
(29) Flint, C. D.; Greenough, P.; Mathews, A. P. *J. Chem. Soc., Faraday Trans. 2* **1973**, *69*, 23–28.

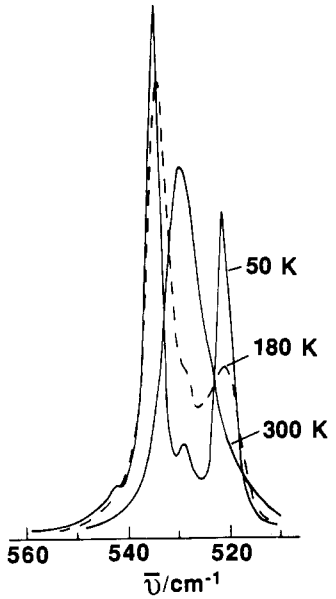

Figure 2. Temperature dependence of the *XX*-polarized Raman spectrum of the $A_1(a_{1g})$ vibration for (+)-2[$Co(en)_3$]Cl_6·NaCl·$6H_2O$.

numbers in parentheses give the potential energy distribution[30] (PED) expressed as a percentage. The coordinates contributing less than 10% to the potential energy are omitted.

The solution Raman spectrum of ±Co shows only four broad bands, at 526 cm^{-1} (A_1), 444 cm^{-1} (E), 376 cm^{-1} (E), and 280 cm^{-1} (A_1 + E). We have measured the RREP of the four bands and obtained essentially the same results as those of Stein et al.[13] The two E vibrations show no resonance effects, while both A_1 bands exhibit a large destructive interference for excitation within the $^1T_1 \leftarrow {}^1A_1$ transition. Our spectroscopic data do not provide any new information, and ref 13 and 18 should be consulted for the observed RREP and absorption spectra.

4. Discussion

4.1. Raman Assignments. If the C–N and C–C stretching vibrations are ignored, then the $M(NCCN)_3$ skeleton with D_3 symmetry should have $4A_1 + 4A_2 + 8E$ vibrations. Of these the highest in energy, A_2 + E, lie above 550 cm^{-1} and involve mainly asymmetric deformations, δ_{NCC}. The lowest in energy, A_2 + E, lie near 100 cm^{-1} and involve torsional motion, τ_{MN}. The remaining vibrations lie in the range 150–550 cm^{-1} and can be classified into the set $3A_1 + 2A_2 + 5E$, derived from the MN_6 skeleton (Table III), and the pair A_1 + E, which involve principally the chelate deformations, τ_{CC} and δ_{MNC}. The Raman spectra (Figures 1, 3, and 4) indicate that this region has 6A + 7E bands, one E mode in excess of the theoretical predictions.

Apart from the congested region, 250–300 cm^{-1}, of the Raman spectra the agreement between the calculated and observed frequencies, as well as deuteriation shifts, is reasonable (Tables IV and V). The largest discrepancies occur for the deuteriation shifts of the $A_1(a_{1g})$ modes and the $A_1(t_{2g})$ mode of ±Rh. The discrepancies for the $A_1(a_{1g})$ modes must be an artifact of our simplified model. The unusually large shift of 43 cm^{-1} attributed to the $A_1(t_{2g})$ mode of ±Rh may not be accurate, as it arises from the comparison of data obtained by different techniques.[14,15]

The Raman spectra near 270 cm^{-1} are partially resolved by the polarization data (Figures 1, 3, and 4) and consist of 2A + 2E bands. The higher energy A band, which lies at 281 cm^{-1} for +Co, is strongly *XX* polarized with very little *ZZ* scattering. It is the main component of the band observed at 280 cm^{-1} in the solution Raman spectrum of $Co(en)_3^{3+}$ [13,27] and must be assigned as A_1 in D_3 symmetry. The overlap with the weaker E bands accounts for the solution depolarization ratio, $\rho_p = 0.16$.[13] According to Tables IV and V, the A_1 band is predominantly the symmetrical δ_{MNC} deformation mode with some t_{2u} and τ_{CC} character.

Two E vibrations are expected to occur near the congested region, $E(t_{2g} + \tau_{MN})$ and $E(\tau_{CC})$. The frequency of the band at 316 cm^{-1} in the spectrum of +Co (Figure 1) is relatively insensitive to the central metal ion, and accordingly this mode is assigned to $E(\tau_{CC})$.

The pair of bands at 284 and 280 cm^{-1} in the spectrum of +Co may represent the two E components arising from $E(t_{2g} + \tau_{MN})$. Both shift by about 30 cm^{-1} to lower energy on going to ±Rh, compared with a predicted shift for $E(t_{2g} + \tau_{MN})$ of ~24 cm^{-1}. Moreover, we note that the unit cell of +Co approaches C_6 symmetry,[19] under which the E modes of the complex ions within the same unit cell will couple to give rise to Raman-active vibrations of $E_1(XZ = YZ)$ and $E_2(XX = XY)$ character (Table III). The pair do indeed show these polarization properties with the E_2-like band lying at higher energy. Similarly, we would predict that the A_1 modes in +Co will have two components that transform as A and B in the approximate C_6 symmetry (Table III). At 50 K (Figures 2 and 3) we do observe two major components for the A_1 (a_{1g}) band, and the weaker component at lower energy may correspond to the B-like mode.

The Raman spectra of ±Co and ±Rh also exhibit separation of polarization intensities for the modes with E_g symmetry (Figures 3 and 4). Our tentative analysis suggests that a higher order pseudosymmetry is also operating for these systems, with the two E_g components showing $E_{1g}(XZ = YZ)$ and $E_{2g}(XX = XY)$ type behavior of the D_{6h} factor group.

The remaining weak band in the congested region occurs at 274 cm^{-1} for +Co and has A symmetry. It is assigned to $A_2(t^a_{1u} + \tau_{MN})$, which becomes allowed in C_3 site symmetry. It corresponds to the strong infrared absorption observed at 280 cm^{-1} for

Table IV. Vibrational Data (cm^{-1}) for $Co(en)_3^{3+}$

	$\bar{\nu}_H$		$\bar{\nu}_H - \bar{\nu}_D$		
D_3	calc	obs[b]	calc	obs[b]	assgnt[a]
A_1	519	529	42	28	a_{1g} (62), δ_{NCC} (13), δ_{CoNC} (11)
	311	350	34	30	t_{2g} (34), τ_{CC} (15), δ_{NCC} (13)
	247	281	7	6	δ_{CoNC} (28), t_{2u} (27), τ_{CC} (12)
	195	212	10	4	t_{2u} (35), t_{2g} (31)
A_2	476	473	20	13	t^b_{1u} (69), δ_{NCC} (16)
	285	274	35	23	t^a_{1u} (43), τ_{CoN} (26), t^b_{1u} (14)
	129		6		τ_{CoN} (51), t^a_{1u} (35)
E	505	504	41	35	t^b_{1u} (66)
	437	446	26	29	e_g (39), t^a_{1u} (14), δ_{CoNC} (13)
	347	375	19	17	e_g (44), t^a_{1u} (18)
	273	316	24	17	τ_{CC} (30), τ_{NC} (13), δ_{NCC} (10)
	286	284, 280	30	19, 17	t_{2g} (46), τ_{CoN} (19)
	168	190	9	6	t_{2u} (74)
	104	142	3	0	τ_{CoN} (49), t_{2g} (19), t^a_{1u} (18)

[a] See text. The deformation and torsion modes are denoted δ and τ, respectively. [b] Taken from crystal Raman spectra of +Co and +Co-d_{12} at 320 K.

Table V. Vibrational Data (cm^{-1}) for $Rh(en)_3^{3+}$

	$\bar{\nu}_H$		$\bar{\nu}_H - \bar{\nu}_D$		
D_3	calc	obs[b]	calc	obs[c]	assgnt[a]
A_1	564	544	43	29	a_{1g} (65), δ_{RhNC} (12)
	297	331	28	43	t_{2g} (24), δ_{NCC} (19), τ_{CC} (19)
	262	279	10	14	δ_{RhNC} (34), t_{2u} (25), a_{1g} (11)
	183	202	11	11	t_{2u} (38), t_{2g} (38)
A_2	438	447	18	12	t^b_{1u} (79), δ_{NCC} (12)
	279	247	35	33	t^a_{1u} (48), τ_{RhN} (30)
	124	106	5	3	τ_{RhN} (46), t^a_{1u} (41)
E	507	509	38	29	t^b_{1u} (36), e_g (27), δ_{RhNC} (13)
	444	444	28	27	t^b_{1u} (38), e_g (36), δ_{NCC} (12)
	351	357	17	22	t^a_{1u} (31), e_g (18), δ_{RhNC} (18)
	278	309	20	11	τ_{CC} (31), δ_{RhNC} (14), τ_{NC} (13)
	266	258, 245	31	...	t_{2g} (31), τ_{RhN} (29)
	167	185	10	9	t_{2u} (76)
	99	120	3	5	τ_{RhN} (43), t^a_{1u} (23), t_{2g} (22)

[a] See text. The deformation and torsion modes are denoted δ and τ, respectively. [b] Taken from crystal Raman spectrum of ±Rh at 320 K. [c] Taken from ref 14–16.

(30) Nakamoto, K. *Infrared and Raman Spectra of Inorganic and Coordination Compounds*, 3 ed.; Wiley: New York, 1978.

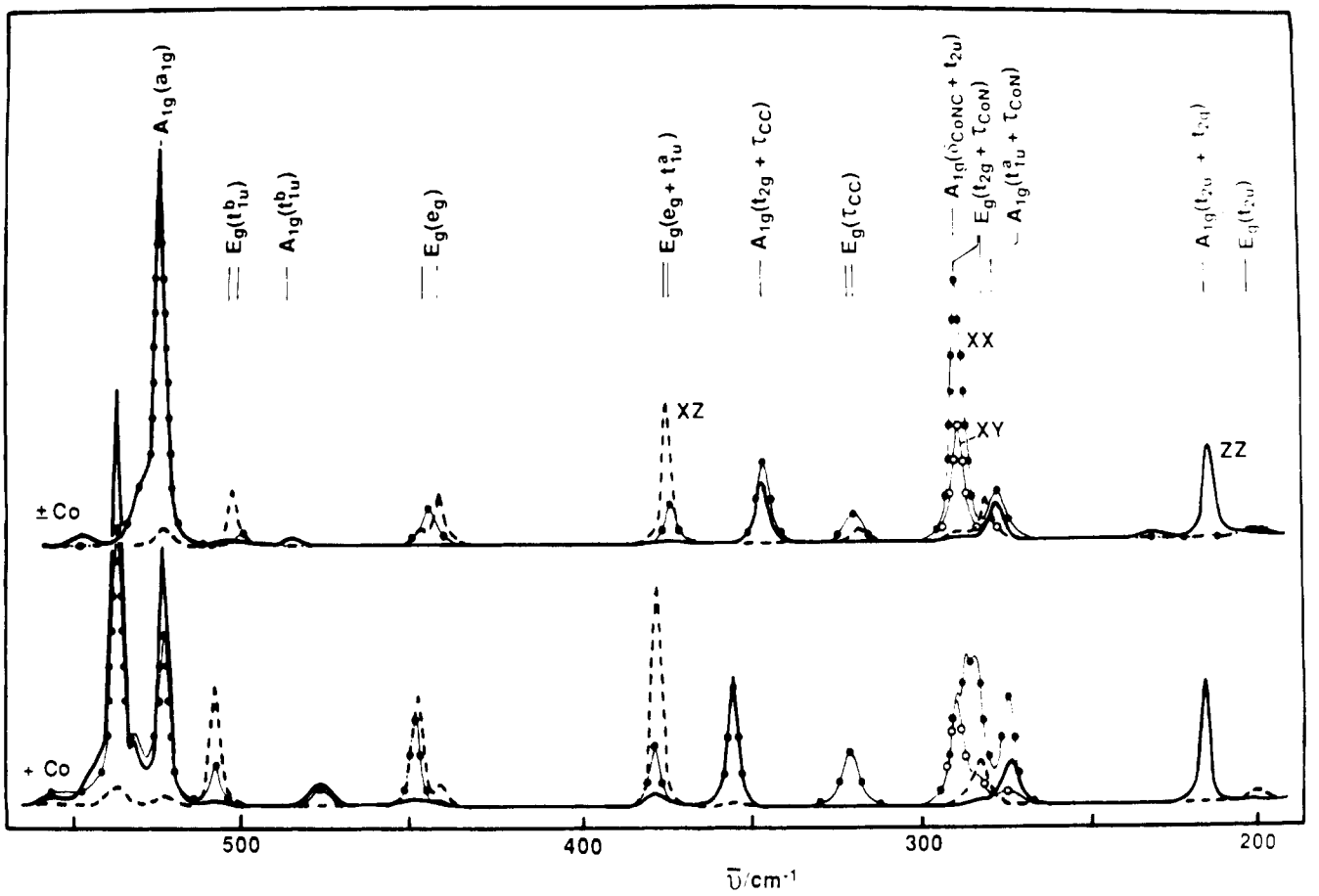

Figure 3. Raman spectra of (±)-2[Co(en)$_3$]Cl$_6$·NaCl·6H$_2$O (±Co) and (+)-2[Co(en)$_3$]Cl$_6$·NaCl·6H$_2$O (+Co) at 50 K. The *XY* spectra have been omitted outside the 250–300-cm^{-1} region. The notation is the same as that used for Figure 1 except that the symmetry species of the D_{3d} factor group of ±Co are used to label the bands.

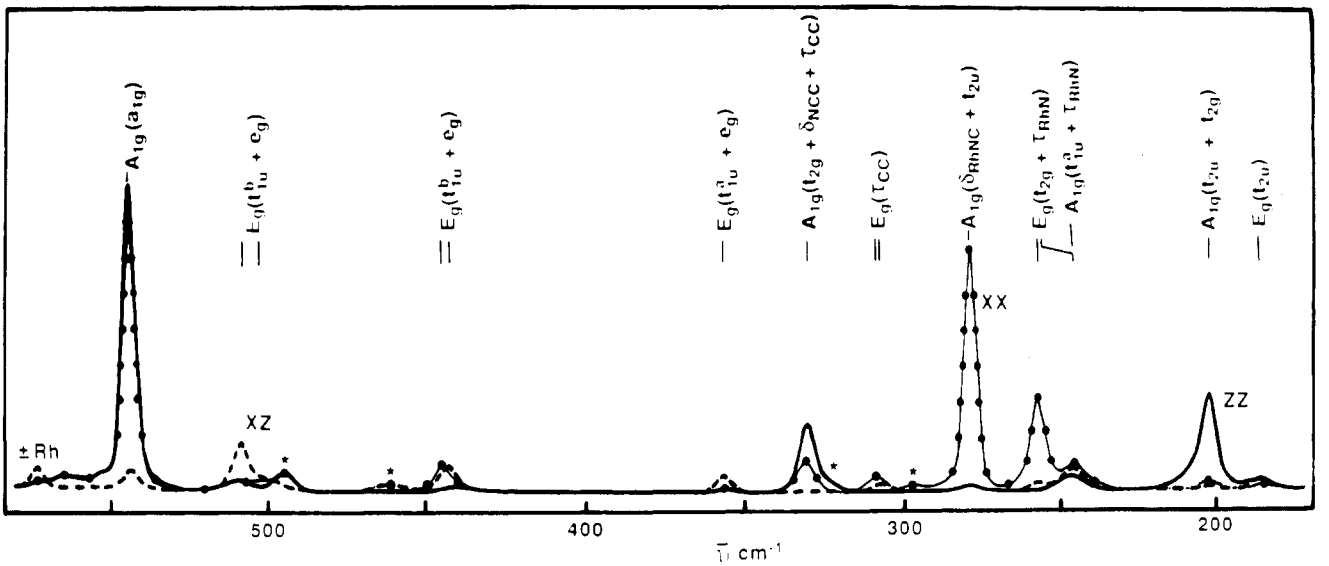

Figure 4. Raman spectrum of 15% (+)-Cr(en)$_3^{3+}$ doped in (±)-2[Rh(en)$_3$]Cl$_6$·KCl·6H$_2$O (±Rh) at ~300 K. Bands due to Cr^{3+} impurity are indicated by asterisks. The notation is the same as that used for Figure 3.

(±)-[Co(en)$_3$]Cl$_3$[10,12] and at 260 cm^{-1} for (±)-[Rh(en)$_3$]Cl$_3$·3H$_2$O.[14]

Our results for A_1 and A_2 vibrations (Tables IV and V) are essentially the same as those of Borch et al.[16] However, there are significant differences for the E vibrations. For example, the E bands near 300 and 444 cm^{-1} for ±Rh were previously assigned[16] to Rh–N stretching and N–Rh–N deformation modes, respectively. In contrast, our calculations assign the 444-cm^{-1} band to E(e_g) and the 309-cm^{-1} band to ligand torsion and deformation modes. These discrepancies are due to errors in E coordinates (section 3.1) and to the selection of observed frequencies. Borch et al.[16] chose ν_{66} = 397 cm^{-1} and ignored the pair of bands that we assign to E(t_{2g} + τ_{RhN}) (Table V) and that were observed by Gouteron[10,12] at 250–260 cm^{-1} in the Raman spectrum of (±)-[Rh(en)$_3$]Cl$_3$·3H$_2$O. The 397-cm^{-1} band was reported as a broad peak in the infrared spectra of polycrystalline samples[14] but was not observed in this work or by Gouteron.[10,12] Its absence in the single-crystal spectra suggest that it may be due to an impurity. For the N,C-perdeuterio complex,[15] ν_{66} was assigned to a Raman-active band at ~400 cm^{-1}. According to our calculations

this band is more likely to correspond to $E(t_{1u}^b + e_g)$.

Our assignments (Tables IV and V) are physically and intuitively realistic. The obvious correspondences between the spectra of $Co(en)_3^{3+}$ and $Rh(en)_3^{3+}$ (Figures 1 and 4) are maintained by the calculations despite the differences in force constants. The only significant differences are for the E modes between 340 and 520 cm^{-1}, which, according to our calculations, constitute admixtures of e_g, t_{1u}^b, and t_{1u}^a. Their actual compositions are quite strongly dependent of the central metal ion, but this is not surprising when it is noted that the relative energies of e_g and t_{1u}^b reverse on going from $Co(NH_3)_6^{3+}$ to $Rh(NH_3)_6^{3+}$.[25,31]

4.2. Resonance Raman Spectrum of $Co(en)_3^{3+}$. The error function model[32-34] is applicable to electronic transitions where the individual vibronic bandwidths are comparable to the energy intervals. For the simple case that involves a single progression building mode, ω_1, and only one Herzberg–Teller active mode, ω_a, the absorption profile for the $^1T_1 \leftarrow {}^1A_1$ transition of $Co(en)_3^{3+}$ is given by[33]

$$A(E_0) \propto \mathrm{Re}[f_1 W(-Z)/\delta_1 + W(-Z')/\delta_1] \quad (3)$$

where W is the complex error function, $Z = (E_m - E_0 - i\Gamma_1)/\delta_1$ and $Z' = Z + \hbar\omega_a/\delta_1$. The first term in (3) represents the profile for a static electric dipole mechanism based on the true origin, $E^0(^1T_1)$. The corresponding Franck–Condon maximum is $E_m = E^0(^1T_1) + S_1\hbar\omega_1$, and f_1 is the ratio of static to vibronic electric dipole strengths. The displacement parameter for the $^1T_1 \leftarrow {}^1A_1$ transition, δ_1, is related to the Huang–Rhys parameter, S_1, by (4).

$$\delta_1^2 = 2(\hbar\omega_1)^2 S_1 \quad (4)$$

The second term in (3) gives the profile for the vibronically induced electric dipole mechanism based on the false origin, $E^0(^1T_1) + \hbar\omega_a$, and $E_m' = E_m + \hbar\omega_a$. The excitation energy is E_0, and the vibronic bandwidth is assumed to be constant with the value Γ_1.

The $^1T_1 \leftarrow {}^1A_1$ absorption band of $Co(en)_3^{3+}$ was modeled by Zgierski[18] using (3) with $f_1 = 0$, $\Gamma_1 = 505$ cm^{-1}, $\hbar\omega_1 = 526$ cm^{-1}, and $\delta_1 = 1683$ cm^{-1}. This analysis ignores the static contribution to the intensity, which must be significant for $Co(en)_3^{3+}$.[1,2] The single-crystal σ absorption and axial CD spectra require $f_1 \approx 0.4$ to account for the large axial CD. The assumption of a single Herzberg–Teller-active mode is obviously not true, and the second term in (3) should be replaced by a sum over all non totally symmetric modes. Similarly, the assumption of a single active A_1 vibration is not justified. Within the error model formalism the latter multimode effect is easily taken into account. Expression 3 is unchanged, but δ_1 should be interpreted as[33]

$$\delta_1^2 = \sum_i \delta_{1i}^2 \quad (5)$$

where the sum is over all active A_1 vibrations. The line shape problem is further complicated by the trigonal splitting of the $^1T_1$ state,[1] anisotropy in σ- and π-polarized intensities,[1] and the fact that (3) strictly applies only at low temperatures.

Although a quantitative study of the solution absorption profile appears to be intractable, Zgierski's analysis[18] is qualitatively reasonable, since his choice of "effective" ω_1 and δ_1 parameters accounts for the bandwidth in solution, $\bar{\nu}_{1/2} \approx 3300$ cm^{-1}. For $f_1 = 0$ and $\Gamma_1/\delta_1 < 0.5$ the profile in (3) has a width at half-height of

$$\bar{\nu}_{1/2} \approx 2(\ln 2)^{1/2}\delta_1 + 1.1\Gamma_1 \quad (6)$$

Furthermore, the value[18] $S_1\hbar\omega_1 = 2692$ cm^{-1} agrees with the Franck–Condon maximum observed in the single-crystal absorption spectra,[1] $E_m \approx E^0(^1T_1) + 2500$ cm^{-1}. The choice of $\Gamma_1 = 505$ cm^{-1} is, however, questionable. It is possible to obtain comparable fits to the absorption spectra with $\Gamma_1 \approx 100$ cm^{-1} and $f_1 \neq 0$ and by slightly increasing the value of δ_1.

Within the error function model[34] we obtain the following expression for the RREP for the jth A_1 vibration in diagonal polarization:

$$I(E_0)_j \propto |f_1(\delta_{1j}/\delta_1)[i\pi^{1/2}Z\,W(-Z) - 1]/\delta_1 + (\delta_{1j}/\delta_1) \times [i\pi^{1/2}Z'\,W(-Z') - 1]/\delta_1 + f_2\delta_{2j}(E_2^2 + E_0^2)/(E_2^2 - E_0^2)^2|^2 \quad (7)$$

The first and second terms in (7) are respectively the resonance scattering amplitudes based on the static and vibronically allowed electric dipole mechanisms. The third term is preresonance Franck–Condon scattering (A term) from an allowed charge-transfer state with displacement δ_{2j} and band maximum at energy $E_2 = E_2^0 + \sum_i S_{2i}\hbar\omega_{2i}$. It is derived by means of the approximation

$$\sum_{k=0}^{\infty}(S^k/k!)[\exp(-S)]f(a + kb) \approx f(a + Sb) \quad (8)$$

The vibronic electric dipole of the $^1T_1 \leftarrow {}^1A_1$ transition is assumed to be derived from this allowed charge transfer, and the corresponding ratio of the dipole strengths is given by f_2. Expression 7 is identical with that of Mejan et al.[34] except for the factors δ_{1j}/δ_1, which take into account the multimode effect for A_1 vibrations.[33] Zgierski's eq 12 in ref 18 does not contain the factors δ_{1j}/δ_1, and the sign of the preresonance scattering amplitude is *incorrect*. Consequently, our conclusions on the signs of the interference term in the RREP and the displacement parameters, δ_{2a_1} and δ_1, will be opposite to those of Zgierski.[18]

The RREP for the $A_1(a_{1g})$ vibration was interpreted by Zgierski[18] using $E_2 = 47400$ cm^{-1}, $f_1 = 0$, $\delta_{1j}/\delta_1 = 1$, $\Gamma_1 = 505$ cm^{-1}, and $f_2\delta_{2j} = 862300$ cm^{-1}.[18] However, since the coordinated chelate ligands cause mixing of the $A_1(a_{1g})$ mode with $A_1(t_{2g})$, $A_1(t_{2u})$, and the A_1 ligand deformation mode at $\sim$280 cm^{-1}, we expect $\delta_{1a_1}/\delta_1 < 1$. This reduces the destructive interference, and in order to restore the fit it is necessary to reduce Γ_1 below the value of 505 cm^{-1}. Although the spectroscopic data are not sufficiently accurate to determine Γ_1 with any precision, a value as low as 100 cm^{-1} seems possible. In crystal absorption spectra at low temperatures, the bandwidth of the origin is only $\sim$30 cm^{-1}.[1]

We can estimate δ_{2a_1} for the charge-transfer transition by using the absorption data of Stein et al.[13] (dipole strength $\propto \epsilon_m\bar{\nu}_{1/2}$), ignoring anisotropy in σ and π dipole strengths and putting $\delta_{1a_1}/\delta_1 \approx 1$. If $f_1 = 0$ or 0.4, we calculate $f_2 = 490$ or 686. If we use $f_2\delta_{2a_1} \approx 8.6 \times 10^5$ cm^{-1} to fit the preresonance part of the profile, we obtain $\delta_{2a_1} = 1760$ or 1260 cm^{-1} and $S_{2a_1} = 5.6$ or 2.9. These are very rough estimates but illustrate the point that S_{2a_1} need not be very large. The charge-transfer state should be subject to strong Jahn–Teller distortion (vide infra), and progressions in the Jahn–Teller-active E vibrations should also contribute significantly to the bandwidth.

Since the $^1T_1 \leftarrow {}^1A_1$ transition involves the one electron jump, $e_g \leftarrow t_{2g}$, there is no question that both δ_{1a_1} and δ_1 have positive signs. Numerical computation shows that the interference between resonance and the preresonance mechanism is destructive provided δ_{2a_1} has the *same* sign as δ_1. The same result obtains for the RREP of an individual vibronic line. Accordingly the higher state must also be expanded along the a_{1g} coordinate.

5. Conclusion

The assignments presented in section 4.1 should provide a sound basis for the interpretation of vibrational structure in the electronic spectra of $M(en)_3$ complexes. The vibronic fine structure in the excited states of ±Rh and ±Co will be examined elsewhere.[36] It will be shown that the skeletal vibrations in the $^4A_{2g}$ state of the $Cr(en)_3^{3+}$ impurity in ±Rh have energies similar to those of ±Co in the excited $^1T_{1g}$ state, thereby confirming many of the earlier assignments made by Denning.[4] The complexity[6,7] of the fine structure associated with the $^2T_1$, $^2E \leftarrow {}^4A_2$ transitions of the

(31) Terrase, J. M.; Poulet, H.; Mathieu, J. P. *Spectrochim. Acta* **1964**, *20*, 305–15.
(32) Mingardi, M.; Siebrand, W. *J. Chem. Phys.* **1975**, *62*, 1074–85.
(33) Van Labeke, D.; Jacon, M.; Berjot, M.; Bernard, L. *J. Raman Spectrosc.* **1974**, *2*, 219–37.
(34) Mejan, T.; Forel, M. T.; Bourgeois, M. T.; Jacon, M. *J. Chem. Phys.* **1980**, *72*, 687–93.
(35) Hitchman, M. A. *Inorg. Chem.* **1982**, *21*, 821–23.
(36) Dubicki, L.; Williamson, B. E.; Harnung, S. E., manuscript in preparation.

$Cr(en)_3^{3+}$ impurity is *not* due to low-energy phonon modes.[7] Zeeman spectra[36] show that some of the fine structure is due to several inequivalent species whose $^2T_1$ energy levels are resolved but the $^2E(R_1,R_2)$ levels coalesce into *one* set of moderately broad R_1 and R_2 lines with bandwidths $\bar{\nu}_{1/2} \approx 3$ cm^{-1}.

The implication of section 4.2, that both the $^1T_1$ excited state and the higher lying charge-transfer state of $Co(en)_3^{3+}$ are expanded along the a_{1g} coordinate, is contrary to the conclusion of earlier workers.[18] Independently of our analysis of the RREP, we *would* expect the excited state associated with the higher energy transition to be expanded along a_{1g}. The intense absorption in $Co(en)_3^{3+}$ at 47 400 cm^{-1} must surely be a charge transfer from the nitrogen atoms to the metal e_g orbitals, e.g. $(e_g)^1(t_{2g})^6(t_{1u})^5 \leftarrow (t_{2g})^6(t_{1u})^6$. The charge separation will tend to shorten the Co–N bonds, but this effect is more than compensated by a large change in crystal field energy. For example, the change in the Co–N bond lengths is approximately

$$\delta R_0 \propto n(-18Dq(Co^{2+}) + 24Dq(Co^{3+})) - e^2/R_0 \quad (9)$$

where we have assumed $Dq \propto 1/R^n$ and $n \approx 5$.[35] We therefore expect the charge-transfer state to be expanded along the a_{1g} coordinate.

Acknowledgment. We thank Dr. Ward Robinson of the University of Canterbury for measuring the unit cell parameters of +Co at ~135 K.

Registry No. $[Co(en)_3]^{3+}$, 14878-41-2; $[Rh(en)_3]^{3+}$, 16786-61-1; D_2, 7782-39-0; $[Co(en)_3]Cl_3$, 13408-73-6; $[Rh(en)_3]Cl_3$, 14023-02-0; $2[Co(en)_3]Cl_6 \cdot 6H_2O$, 15004-81-6; (+)-$Cr(en)_3^{3+}$, 41509-53-9; (±)-$Cr(en)_3^{3+}$, 15276-13-8.

Contribution from the Department of Chemistry, University of Illinois at Chicago, Chicago, Illinois 60680, and Institut für Anorganische und Angewandte Chemie der Universität Hamburg, D-2000 Hamburg 13, Federal Republic of Germany

Effects of Rovibrational Averaging on the ^{93}Nb Chemical Shift in the $[Nb(CO)_6]^-$ Ion, Based on NMR and Vibrational Spectra

Cynthia J. Jameson,*[1a] Dieter Rehder,*[1b] and Martin Hoch[1b]

Received October 8, 1987

We report the dependence of the ^{93}Nb NMR spectrum of $[Nb(CO)_6]^-$ in solution upon temperature (203–323 K) and upon isotopic replacement of $^{12}C^{16}O$ ligands by $^{13}C^{16}O$ and $^{12}C^{18}O$. The IR and Raman spectra of the hexacarbonyl anion are reported for the solid $[Et_4N]^+[Nb(CO)_6]^-$. In a comparative study of $[V(CO)_6]^-$, $[Nb(CO)_6]^-$, and $[Re(CO)_6]^+$ ions, force constants are calculated in a general quadratic valence force field constrained to be consistent with the interaction force constants in the corresponding neutral hexacarbonyl series $Cr(CO)_6$, $Mo(CO)_6$, and $W(CO)_6$. The harmonic force field augmented with estimated anharmonic force constants is used to calculate mean NbC and CO bond displacements as a function of temperature and masses. The ^{93}Nb chemical shifts upon isotopic CO replacement are interpreted in terms of rovibrational averaging, and the empirical values of the electronic factors so obtained are found to be consistent with the observed temperature dependence of the shift.

Introduction

The temperature dependence[2–6] and isotope effects[5,7–12] of chemical shifts of transition-metal nuclei in diamagnetic complexes are very large compared to those for other nuclei (roughly in correlation to their ranges of chemical shifts).[13] We have shown that in the prototypical cases $[V(CO)_6]^-$ and $[Co(CN)_6]^{3-}$ the observed temperature coefficients of the ^{51}V and ^{59}Co chemical shifts in these complexes in solution can be attributed largely to the increase in the vibrationally averaged metal–ligand distance with increase in temperature rather than the decreased intermolecular effects on liquid expansion with temperature.[5] The chemical shifts due to isotopic replacement ($^{13/12}$C, $^{18/16}$O, and $^{15/14}$N) of neighboring atoms in these complexes have been interpreted consistently with the same rovibrational averaging model used for the temperature coefficients.

In this paper we report temperature dependence and isotope effects of ^{93}Nb chemical shifts in $[Nb(CO)_6]^-$, in a continuing study of trends in the low-spin d^6 metal hexacarbonyl ions. We measured the infrared and Raman spectra of $[Nb(CO)_6]^-$ and provide a harmonic force field analysis for this complex that is consistent within the series of neutral hexacarbonyls $M(CO)_6$ (M = Cr, Mo, W)[14] and the hexacarbonyl ions $[M(CO)_6]^-$ (M = V, Nb) and $[Re(CO)_6]^+$. We used the quadratic force constants from this analysis with an anharmonic model used previously[15] to calculate mean bond displacements and mean square amplitudes in $[Nb(CO)_6]^-$ ion. These are used to interpret the NMR data. The results for ^{93}Nb are compared with those found previously for ^{51}V.

Experimental Section

Sample Preparation. $Na[Nb(CO)_6]$ was prepared by normal-pressure carbonylation of $NbCl_5$ with a Mg/Zn reductant[30] and converted to the more stable $[Et_4N][Nb(CO)_6]$ by treatment with $[Et_4N]Br$ in H_2O/CH_3OH (1/1), where $[Et_4N][Nb(CO)_6]$ is only sparingly soluble. For CO replacement, a 0.025 M solution, prepared under N_2 in highly purified THF, was cooled to 195 K (dry ice/ethanol) and irradiated for 20 min (high-pressure mercury lamp, 125 W) to yield red-violet $[Nb(CO)_5THF]^-$. After removal of the N_2/CO atmosphere via a vacuum line and injection of ^{13}CO or $C^{18}O$, respectively, the solution was warmed to 210 K and shaken, until the yellow color of the (hexacarbonyl)niobate was restored. Five more cycles of THF/CO replacement gave a sample that was 70% isotopically enriched. After filtration of small amounts of decomposition products, the solution was evaporated to dryness and the residue redissolved, for NMR measurements, in 3 mL of acetone-d_6.

(1) (a) University of Illinois. (b) Universität Hamburg.
(2) Benedek, G. B.; Englman, R.; Armstrong, J. A. *J. Chem. Phys.* **1963**, *39*, 3349–3363.
(3) Brown, T. H.; Cohen, S. M. *J. Chem. Phys.* **1973**, *58*, 395–396.
(4) Rehder, D. *Bull. Magn. Reson.* **1982**, *4*, 33–83.
(5) Jameson, C. J.; Rehder, D.; Hoch, M. *J. Am. Chem. Soc.* **1987**, *109*, 2589–2594.
(6) Jameson, C. J.; Jameson, A. K.; Herlinger, A., to be submitted for publication.
(7) McFarlane, H. C. E.; McFarlane, W.; Rycroft, D. S. *J. Chem. Soc., Dalton Trans.* **1976**, 1616–1622.
(8) Bendall, M. R.; Doddrell, D. M. *Aust. J. Chem.* **1978**, *31*, 1141–1143.
(9) Näumann, F.; Rehder, D.; Pank, V. *J. Organomet. Chem.* **1982**, *240*, 363–369.
(10) Harris, R. K.; Morrow, R. J. *J. Chem. Soc., Faraday Trans.* **1984**, *80*, 3071–3094.
(11) Russell, J. G.; Bryant, R. G.; Kreevoy, M. M. *Inorg. Chem.* **1984**, *23*, 4565–4567.
(12) Hoch, M.; Rehder, D. *Inorg. Chim. Acta* **1986**, *111*, L13–L15.
(13) Jameson, C. J.; Osten, H. J. *Ann. Rep. NMR Spectrosc.* **1986**, *17*, 1–78.
(14) Jones, L. H.; McDowell, R. S.; Goldblatt, M. *Inorg. Chem.* **1969**, *8*, 2349–2363.
(15) Jameson, C. J. *J. Am. Chem. Soc.* **1987**, *109*, 2586–2588.

0020-1669/88/1327-3490$01.50/0